Received: 21 March 2022 | Revised: 26 May 2022 | Accepted: 3 June 2022

DOI: 10.1002/pld3.415

ORIGINAL RESEARCH

Identification of BAHD acyltransferases associated with acylinositol biosynthesis in *Solanum quitoense* (naranjilla)

Bryan J. Leong[1,2] | Steven Hurney[3,4] | Paul Fiesel[5] | Thilani M. Anthony[5] | Gaurav Moghe[5,6] | Arthur Daniel Jones[3,5] | Robert L. Last[1,5]

[1]Department of Plant Biology, Michigan State University, East Lansing, Michigan, USA

[2]Horticultural Sciences Department, University of Florida, Gainesville, Florida, USA

[3]Department of Chemistry, Michigan State University, East Lansing, Michigan, USA

[4]Michigan Department of Health and Human Services, Lansing, Michigan, USA

[5]Department of Biochemistry and Molecular Biology, Michigan State University, East Lansing, Michigan, USA

[6]Plant Biology Section, School of Integrative Plant Sciences, Cornell University, Ithaca, New York, USA

Correspondence
Robert L. Last, Department of Plant Biology, Michigan State University, East Lansing, MI, USA.
Email: lastr@msu.edu

Present address
Bryan J. Leong, Horticultural Sciences Department, University of Florida, Gainesville, Florida, USA

Steven Hurney, Michigan Department of Health and Human Services, Lansing, Michigan, USA

Gaurav Moghe, Plant Biology Section, School of Integrative Plant Sciences, Cornell University, Ithaca, New York, USA

Funding information
USDA National Institute of Food and Agriculture, Grant/Award Number: MICL02474; National Institutes of Health, Grant/Award Number: T32-GM110523; National Science Foundation, Grant/Award Number: IOS-PGRP-1546617

Abstract

Plants make a variety of specialized metabolites that can mediate interactions with animals, microbes, and competitor plants. Understanding how plants synthesize these compounds enables studies of their biological roles by manipulating their synthesis in vivo as well as producing them in vitro. Acylsugars are a group of protective metabolites that accumulate in the trichomes of many Solanaceae family plants. Acylinositol biosynthesis is of interest because it appears to be restricted to a subgroup of species within the Solanum genus. Previous work characterized a triacylinositol acetyltransferase involved in acylinositol biosynthesis in the Andean fruit plant *Solanum quitoense* (lulo or naranjilla). We characterized three additional *S. quitoense* trichome expressed enzymes and found that virus-induced gene silencing of each caused changes in acylinositol accumulation. pH was shown to influence the stability and rearrangement of the product of ASAT1H and could potentially play a role in acylinositol biosynthesis. Surprisingly, the in vitro triacylinositol products of these enzymes are distinct from those that accumulate *in planta*. This suggests that additional enzymes are required in acylinositol biosynthesis. These characterized *S. quitoense* enzymes, nonetheless, provide opportunities to test the biological impact and properties of these triacylinositols in vitro.

1 | INTRODUCTION

Plant specialized metabolites are taxonomically-restricted small molecules that mediate a variety of interactions with the environment (Howe & Jander, 2008; Massalha et al., 2017; Mithöfer & Boland, 2012). These include protection from deleterious microbes and herbivores (Ahuja et al., 2012; Howe & Jander, 2008) and abiotic stresses such as UV-B (Landry et al., 1995), as well as interactions with beneficial bacterial and fungal partners, including symbionts (Massalha et al., 2017) and pollinators (Stevenson et al., 2017). Despite their diverse structures and sometimes complex biosynthesis, specialized metabolites are often made from simple components such as amino acids, sugars, and fatty acids as well as core metabolic intermediates.

Acylsugars are a class of specialized metabolites produced across the Solanaceae family (Fan et al., 2019; Moghe et al., 2017). These molecules contain a sugar core modified by esterification with one or more acyl groups. The acyl chains are derived from fatty acid and amino acid metabolism with strong intraspecific diversity (Fan et al., 2020; Kim et al., 2012; Landis et al., 2021; Mandal et al., 2020; Ning et al., 2015); they range from 2 to 20 carbons in length with straight or branched configurations (Fan et al., 2019; Herrera-Salgado et al., 2005). Many acylsugars contain a sucrose core (Ghosh et al., 2014; King et al., 1986; Liu et al., 2017; Maldonado et al., 2006; Moghe et al., 2017), while others produce acylhexoses, including glucose and inositol (Burke et al., 1987; King & Calhoun, 1988; Matsuzaki et al., 1989). One example is the wild tomato *Solanum pennellii* (LA0716), which uses an invertase-like enzyme to convert acylsucroses to acylglucoses (Leong et al., 2019; Lybrand et al., 2020). Another is the black nightshade *Solanum nigrum*, a Solanaceae species from the eastern hemisphere (also referred to as the "Old World") that uses a phylogenetically distinct invertase-like enzyme to synthesize acylglucoses (Lou et al., 2021).

Enzymes of various classes were demonstrated to play roles in acylsugar biosynthesis. The sugar acylating enzymes are clade III BAHD (named after the first four enzymes of this class) acyltransferases known as acylsugar acyltransferases (ASATs), which modify sugar cores using Coenzyme A thioesters as acyl group donors (Fan et al., 2016; Moghe et al., 2017; Nadakuduti et al., 2017; Schilmiller et al., 2015). Previous publications described characterization of ASATs across the Solanaceae: in cultivated (*Solanum lycopersicum*) and wild tomato species (e.g., *S. pennellii*) (Fan et al., 2017; Schilmiller et al., 2012, 2015), *S. nigrum* (Lou et al., 2021), *Petunia axillaris* (Nadakuduti et al., 2017), and *Salpiglossis sinuata* (Moghe et al., 2017). Trichome-expressed variants of primary metabolic enzymes, including isopropylmalate synthase, enoyl-CoA hydratase, and CoA ligase, provide ASAT acyl CoA substrates in cultivated tomato and *S. quitoense* (Fan et al., 2020; Ning et al., 2015). In addition, acylsugar hydrolases that remove acyl chains were identified, but their biosynthetic roles are as yet undefined (Ghosh et al., 2014; Schilmiller et al., 2016). These enzymes play distinct roles in acylsugar biosynthesis.

The presence of acylinositols in *S. quitoense*, *S. nigrum*, and *Solanum lanceolatum* offers an opportunity to study acylsugar core diversity in the *Solanum* clade (Herrera-Salgado et al., 2005; Leong et al., 2020). While members of the Leptostemonum clade—the largest monophyletic clade in the *Solanum* genus—were not thoroughly explored in a previous survey of acylsugars across the Solanaceae family (Moghe et al., 2017), *S. quitoense* and *S. lanceolatum* both produce acylated inositols. *S. quitoense* acylinositols with acyl chains of 2, 10, and 12 carbons on a *myo*-inositol core are the major acylsugars (Figure S1), along with less abundant acylinositol glycosides (Hurney, 2018; Leong et al., 2020). *S. lanceolatum* acylinositol glycosides primarily have an acyl chain from 12 to 20 carbons (Herrera-Salgado et al., 2005). Only one acylsugar acyltransferase has been described in either of these species: a triacylinositol acetyltransferase (TAIAT) that synthesizes tetraacylinositols in *S. quitoense* (Leong et al., 2020). This system presents an opportunity to understand how acylsugar pathways diverged in the *Solanum* clade.

We sought to identify other BAHD acyltransferases involved in acylinositol biosynthesis based upon characteristics of known ASATs. These include phylogenetic relationships, presence of conserved domains, and enriched glandular trichome expression (Leong et al., 2020). Here we report the identification of three tomato ASAT homologs: SqASAT1H, SqASAT3H, and a homolog of ASAT4 (SqASAT4H). Consistent with roles in acylinositol metabolism, virus-induced gene silencing (VIGS) of each candidate caused alteration of acylinositol quantity or acylation pattern. Screening recombinant ASATs in vitro demonstrated that ASAT1H acylated *myo*-inositol using nC10- and nC12-CoA, which are chains that match *in planta* products ("n" signifying straight chain). The ASAT1H substrate affinity for sugars and acyl-CoAs matches other ASATs. However, we found that ASAT1H in vitro acylation position does not match *in planta* products. This may be due to in vivo rearrangement of the monoacylinositol, which has been previously described in vitro for monoacylsucroses (Fan et al., 2016; Lou et al., 2021). ASAT4H and ASAT3H acylate the original monoinositol and subsequent diacylinositol to generate diacylinositols and triacylinositols, respectively. Contrary to expectation, the resulting triacylinositols do not co-elute with the *in planta* product.

2 | RESULTS AND DISCUSSION

2.1 | Candidate gene identification

We sought acylinositol biosynthetic enzymes by screening for trichome-expressed BAHD acyltransferases that are phylogenetically related to characterize ASATs (Figure 1). We employed the same criteria used to identify TAIAT (Leong et al., 2020): seeking candidates with ≥500 reads in trichome RNAseq samples, predicted to encode proteins 400–500 amino acids in length with the canonical BAHD motifs HXXXD and DFGWG present in proper orientation (DAuria, 2006). Three transcripts assemblies met these criteria:

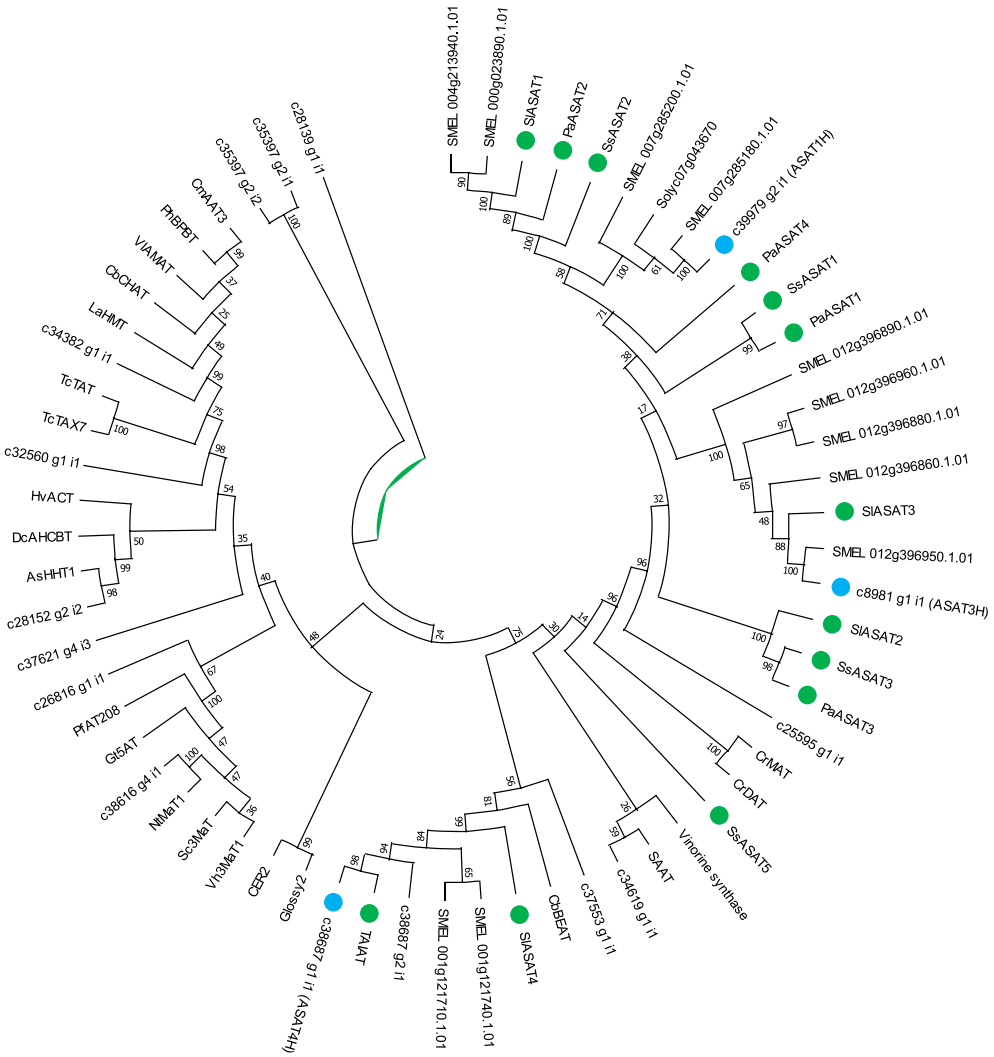

FIGURE 1 Phylogenetic analysis of known BAHD acyltransferases and *Solanum quitoense* acylsugar acyltransferases (ASAT) candidates. Previously characterized ASATs are marked by green circles, while the enzymes described in this study are marked by blue circles. Protein sequences were aligned using MUSCLE with default parameters in MEGA X

TABLE 1 Trichome and shaved petiole RNA-seq data for tested *Solanum quitoense* acylsugar acyltransferase candidates

Transcript name	Average trichome reads	Average petiole reads
c8981_g1_i1	906	2.5
c38687_g1_i1	1633.5	3.3
c39979_g2_i1	4694.5	11.5

Source: Data are derived from Moghe et al. (2017).

c39979_g2_i1, c38687_g1_i1, and c8981_g1_i1. Expression of all three candidates was enriched in *S. quitoense* trichomes relative to the trichome-denuded petiole tissue (Table 1) (Moghe et al., 2017). The first candidate—*c39979_g2_i1* (named ASAT1H below)—is a homolog of both the first enzyme of cultivated tomato acylsucrose biosynthesis, *Sl-ASAT1*, and the *S. lycopersicum* chromosome 7 *Sl-ASAT1* paralog *Solyc07g043670* (Leong et al., 2020; Moghe et al., 2017). The second candidate is the Sl-ASAT3 homolog *c8981_g1_i1* (referred to below as ASAT3H), while *c38687_g1_i1* (ASAT4H) is a paralog of the recently described TAIAT (Leong et al., 2020).

2.2 | In vivo analysis of acylsugar acyltransferase candidates

A previously developed *S. quitoense* VIGS method was employed to test the impact of downregulating the expression of these candidates in vivo (Figure S2). Qualitatively similar results were obtained for each of the two distinct fragments targeting ASAT1H, ASAT3H, or ASAT4H transcripts.

VIGS of all three candidates yielded acylsugar phenotype perturbations. Targeting ASAT1H, ASAT3H, and ASAT4H individually caused reductions in the four major acylinositols (Figure 2a,b, Tables S1 and S2). This phenotype is reminiscent of results from CRISPR knockout lines of ASATs in *S. lycopersicum* and *S. pennellii*, as well as VIGS of *P. axillaris*, *S. sinuata*, *S. nigrum* (Lou et al., 2021), and *S. quitoense* ASATs (Fan et al., 2016; Leong, 2019; Moghe et al., 2017; Nadakuduti et al., 2017; Schilmiller et al., 2015). Real-time quantitative reverse transcription polymerase chain reaction (qRT-PCR) analysis confirmed reductions in candidate transcript abundance in target plants relative to the controls, with three of six constructs significant at $p < .05$ (Figures S3 and S4). The decreased acylsugar accumulation suggests a

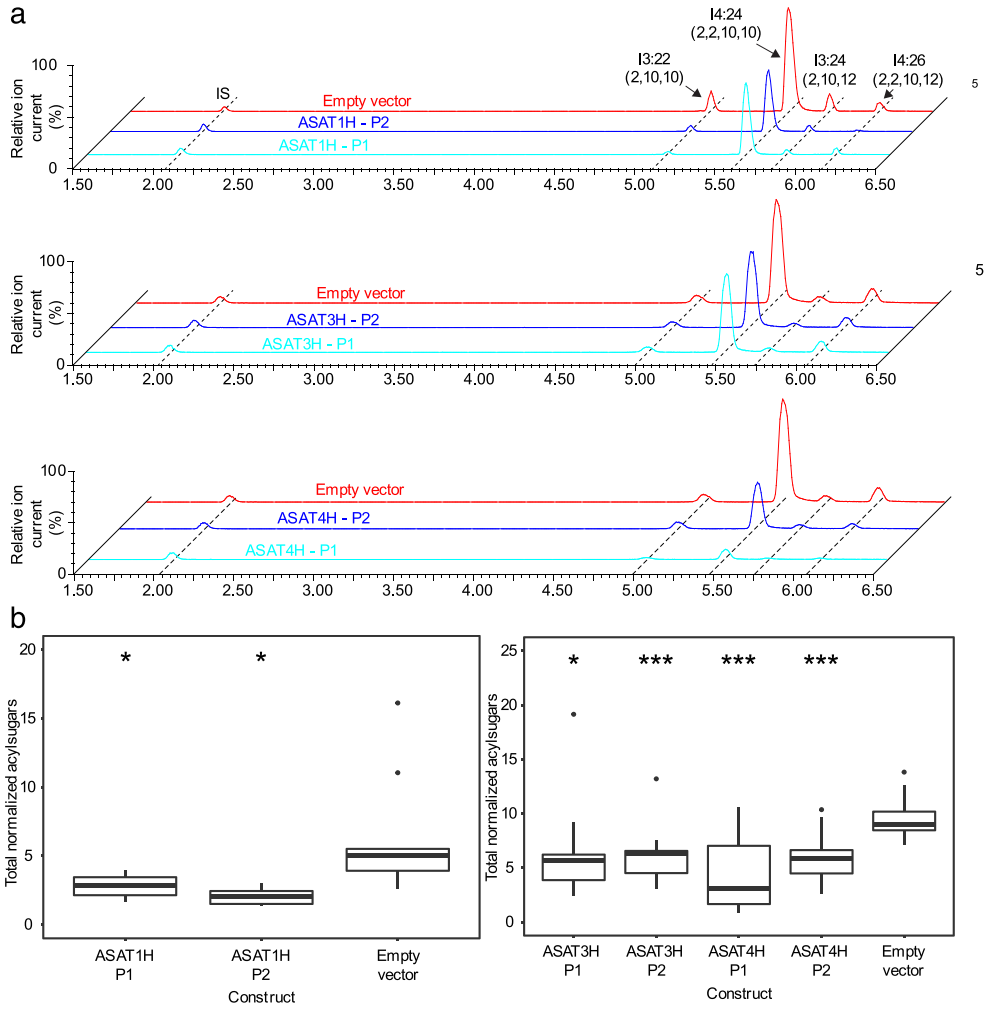

FIGURE 2 Virus-induced gene silencing (VIGS) analysis of acylinositol biosynthesis candidates. (a) Liquid chromatography–mass spectrometry (LC–MS) analysis of acylsugars in ASAT1H, ASAT3H, and ASAT4H-targeted plants from similar sized leaves (<0.6 mg difference). The combined extracted ion chromatogram shows minute 1.50 to 6.50 of a 7 minute method with telmisartan (internal standard), I3:22 (2,10,10), I4:24 (2,2,10,10), I3:24 (2,10,12), and I4:26 (2,2,10,12). Chromatograms combined signals: $[M-H]^-$ for telmisartan and $[M + \text{formate}]^-$ for the acylsugars. The *m/z* values of compounds included in this figure are as follows: telmisartan (internal standard), *m/z* 513.23; I3:22 (2,10,10), *m/z* 577.35; I4:24 (2,2,10,10), *m/z* 619.37; I3:24 (2,10,12), *m/z* 605.4; I4:26 (2,2,10,12), *m/z* 647.4, each with a mass window of 0.05 Da. (b) Total acylsugar boxplots in ASAT1H, ASAT3H, and ASAT4H VIGS samples. Welchs two-sample *t* test was used for pairwise statistical analysis to empty vector controls. Whiskers represent minimum and maximum values less than 1.5 times the interquartile range from the first and third quartiles, respectively. Values outside of this range are depicted using black dots. $^*p < .05$, $^{**}p < .01$, and $^{***}p < .001$. For ASAT1H, ASAT3H, ASAT4H-targeted plants ($n = 14$–15), for ASAT1H empty vector plants ($n = 9$), and for ASAT3H and ASAT4H empty vector plants ($n = 14$)

role in acylinositol biosynthesis and the case for ASAT1H and ASAT3H is bolstered by a lack of other significant paralogs or homology to other candidates that could result in cross-silencing. Targeting ASAT4H—but not ASAT1H or ASAT3H—yielded an increased ratio of monoacetylated triacylinositols to diacetylated tetraacylinositols (Figure S5, Tables S1 and S2). We hypothesized that the similarity between TAIAT and ASAT4H (93% nucleotide identity) could cause cross-silencing (Table S3, Figure S6); this was validated by qRT-PCR analysis, which revealed that targeting ASAT4H caused reduced TAIAT transcript abundance (Figure S4). Thus, TAIAT cross-silencing could have contributed to the reduction in tetraacylinositols that contained two acetate esters. The perturbation of acylinositol accumulation led us to further characterize these candidates using in vitro biochemistry.

2.3 | In vitro analysis of ASAT1H

ASAT1H emerged as the top candidate for the first step in acylinositol biosynthesis based on its amino acid similarity (44% amino acid identity) and phylogenetic relationship to Sl-ASAT1—the enzyme that acylates sucrose in cultivated tomato acylsucrose biosynthesis (Figure 1, Table S3) (Fan et al., 2016)—as well as VIGS-mediated reduction in total acylinositols. We used in vitro biochemistry to determine

whether an *Escherichia coli*-expressed ASAT1H acylates *myo*-inositol using nC10 and nC12-CoA as substrates. These acyl donors were tested because *S. quitoense* trichome acylsugars contain acylinositols esterified with nC10 and nC12 acyl groups (Leong et al., 2020). To minimize rearrangement of the primary products, assays were performed at pH 6 (Fan et al., 2016). Indeed, ASAT1H catalyzed formation of monoacylated inositol using both nC10 and nC12-CoAs and inositol as substrates (Figure 3a). Mass spectrometric analysis using negative-ion mode collision-induced dissociation yielded *m/z* 171.14 or 199.17 fragment ions, values consistent with negatively charged carboxylates of nC10 or nC12 acyl chains, respectively (Figure S7).

We posited that if ASAT1H is involved in acylinositol biosynthesis, it would have donor and acceptor substrate affinities similar to other ASATs (Fan et al., 2016; Schilmiller et al., 2015). Indeed, the apparent K_m for *myo*-inositol with nC10-CoA was 4.4 ± 1.1 mM (95% confidence interval using standard error) (Figure S8 and Table S4), which is similar to the Sl-ASAT1 apparent K_m for sucrose of 2.3 mM (Fan et al., 2016). The apparent K_m of ASAT1H for nC10-CoA and nC12-CoA with *myo*-inositol were 9.5 ± 2.4 μM and 16.6 ± 6.6 μM, respectively. These match the previously reported values for acyl-CoAs of 2–50 μM for Sl-ASAT1, SlASAT2, and ASAT3 enzymes from multiple species (Fan et al., 2016; Schilmiller et al., 2015). Taken together, the ASAT1H apparent K_m donor and acceptor substrate results match other ASATs, consistent with a possible role in acylinositol biosynthesis.

We resolved the I1:10 monoacylinositol product of the reaction of nC10-CoA and *myo*-inositol using nuclear magnetic resonance (NMR) and compared the acylation position with *in planta* acylsugars. I1:10 describes a *myo*-inositol core with one acyl chain of ten carbons; with more than one acyl chain, the numbers of carbon atoms of individual chains are included in parentheses (e.g., I3:22 (2,10,10)). ASAT1H generated a single I1:10 product in reactions run at pH 6, a condition that previously yielded monoacylsucrose esterified at the 4-position with tomato SlASAT1 (Figure 3b) (Fan et al., 2016). Analysis of the purified I1:10 NMR spectra revealed the product to be acylated at the *myo*-inositol 4/6 position (Figures 3c,d and S9 and Tables S5 and S6). This result was unexpected because NMR-resolved structures of *S. quitoense* acylsugars contain nC10 or nC12 acyl chains at the 2- and 1-/3-positions of *myo*-inositol, without evidence of 4-position acylation (Hurney, 2018; Leong et al., 2020). Note

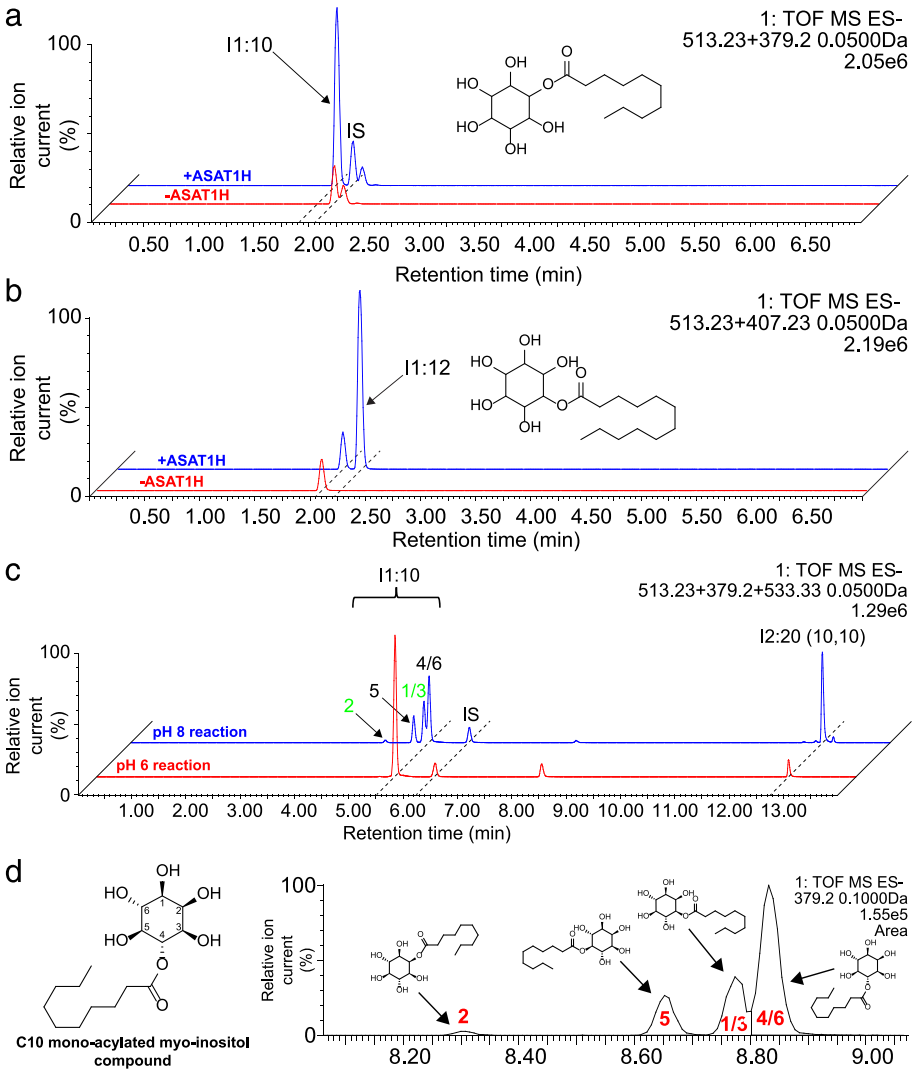

FIGURE 3 ASAT1H in vitro assay product characterization. Liquid chromatography–mass spectrometry (LC–MS) analysis of ASAT1H in vitro assay using *myo*-inositol and (a) nC10-CoA or (b) nC12-CoA. The combined extracted ion chromatogram includes telmisartan (internal standard), I1:10, or I1:12. (c) LC–MS analysis of ASAT1H assays at pH 6 (red) and 8 (blue). The combined extracted ion chromatogram includes telmisartan (internal standard), I1:10, and I2:20 (10,10). I1:10 isomers are labeled and in vivo positions of medium acyl chains are green. (d) Nuclear magnetic resonance (NMR)-derived structure of ASAT1H I1:10 product (left). The extracted ion chromatogram shows relative elution order of monoacylinositol isomers using reverse-phase chromatography on 14-min method with a 0.1-Da mass window (right). The *m/z* values of the compounds in this figure are as follows: telmisartan (internal standard), *m/z* 513.23; I1:10, *m/z* 379.20; I1:12, *m/z* 407.23; I2:20 (10,10), *m/z* 533.33, each with a mass window of 0.05 Da unless otherwise described. All acylsugars are shown as formate adducts

acylations at that *myo*-inositol positions 1/3 and 4/6 are mirror plane symmetrical, and thus indistinguishable by NMR and reverse-phase liquid chromatography (LC). These results show that the in vitro I1:10 does not match *in planta* acylsugars.

In contrast to the pH 6 assay product, we found a mixture of four chromatographically distinct I1:10 *myo*-inositol isomers in reactions at pH ≥7 (Figure 3c). ^{1}H-NMR analysis revealed four monoacylinositol positional isomers at relative peak integration of 2:15:19:64, correlating well with the liquid chromatography–mass spectrometry (LC-MS) peak area ratios of approximately 2:15:22:61 (Figures 3c,d and S10a,b and Table S6). Therefore, we inferred that the monoacylinositol I1:10 esterified at Position 2 eluted first, followed by that at Position 5, Position 1/3, and finally Position 4/6.

As ASAT1 in vitro enzyme assays run at pH 6 and pH 8 produced different product profiles (Figure 3c), we tested the hypothesis that rearrangement of the 4-position monoacylinositol primary product to Position 2 or 1/3 contributes to in vivo biosynthesis. If rearrangement is occurring, the isomers esterified at positions other than 4 should increase with reaction time at pH 8. Indeed, the other isomers, absent at pH 6, increased in abundance over the course of an hour after a shift to pH 8, along with a peak matching the *m/z* of the diacylated compound I2:20 (10,10) (*m/z* 533.33) (Figure S11). Some of these isomers matched the position of medium chains from *in planta* acylsugars. Rearrangement did not require presence of the enzyme, as incubation of purified 4-position ester I1:10 product without enzyme at pH 8 for 60 min at 30°C yielded rearranged I1:10 isomers (Figure S12). We asked whether the rearrangement of the R4 acyl chain was intermolecular or intramolecular by comparing rate and extent of rearrangement following serial dilution. First-order kinetics were obtained, consistent with intramolecular rearrangement: Up to a 9-fold dilution did not impact product formation over 30–60 min (Figure S13). Taken together, these results indicate that a single R4 monoacylinositol is formed in vitro at pH 6 and rearranges non-enzymatically at pH 8. This is reminiscent of the Sl-ASAT1 and SnASAT1 R4 monoacylated sucrose product rearrangement to form R6 monoacylated sucrose at pH ≥7 (Fan et al., 2016) (Lou et al., 2021). Although the absence of acylsugars with acyl groups in the 6-position in tomato and *S. nigrum* strongly suggests that rearrangement is not part of acylsugar biosynthesis in these plants (Fan et al., 2016; Lou et al., 2021), we cannot rule out a role of intramolecular rearrangement in acylinositol metabolism.

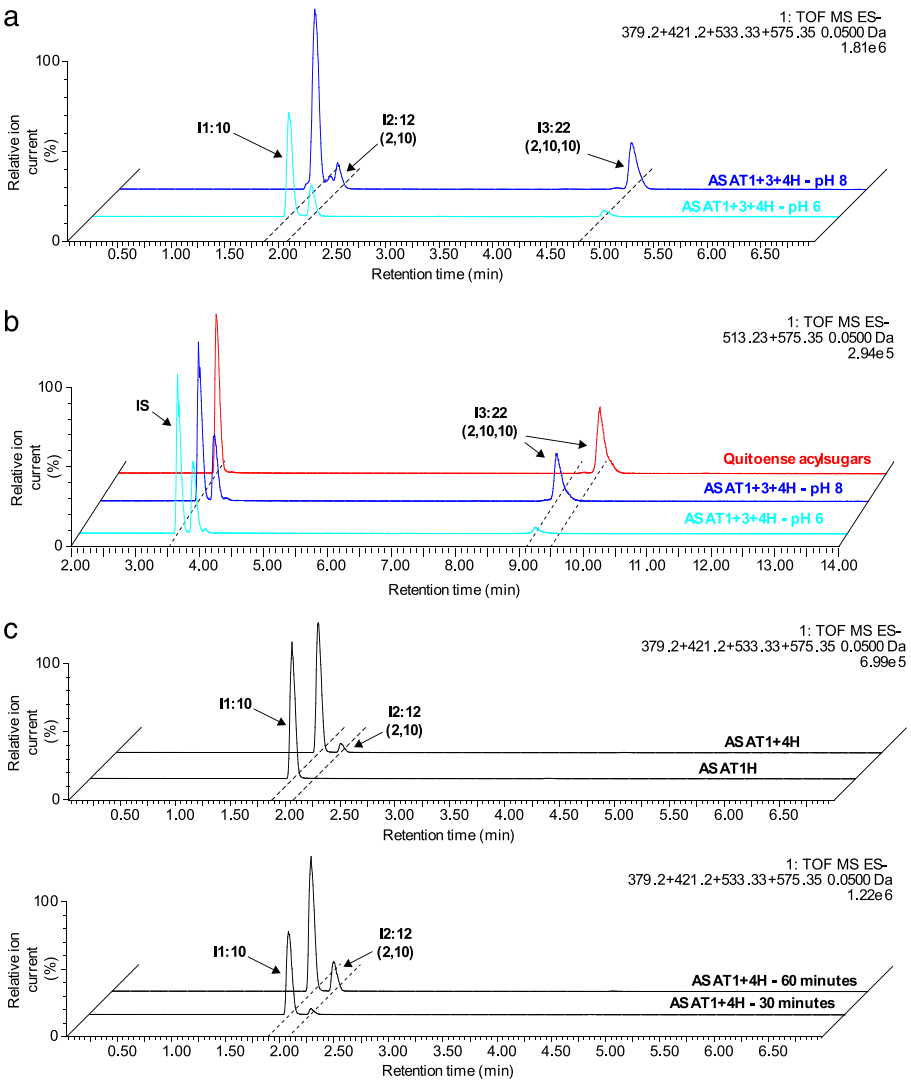

FIGURE 4 ASAT1H, ASAT3H, and ASAT4H in vitro assay product characterization. (a) Liquid chromatography–mass spectrometry (LC–MS) analysis of combined assays with ASAT1H, ASAT3H, and ASAT4H using *myo*-inositol, nC10-CoA and C2-CoA at pH 6 (light blue) or 8 (blue). The combined extracted ion chromatogram includes I1:10, I2:12 (2,10), I2:20 (10,10), and I3:22 (2,10,10). (b) LC–MS analysis of *Solanum quitoense* acylsugars (red), and ASAT1H, ASAT3H, and ASAT4H combined assays using *myo*-inositol, nC10-CoA and C2-CoA at pH 6 (light blue) or 8 (blue) using 21-minmethod. The combined extracted ion chromatogram includes telmisartan (internal standard) and I3:22 (2,10,10). (c) LC–MS analysis of ASAT1H and ASAT4H combined assays using *myo*-inositol, nC10-CoA and C2-CoA at pH 6. Combined extracted ion chromatogram of a 30-minreaction includes I1:10, I2:12 (2,10), I2:20 (10,10), and I3:22 (2,10,10) (top) with reaction progress at 30 and 60 min (bottom). The *m/z* values of the compounds included in this figure are as follows: telmisartan (internal standard), *m/z* 513.23; I1:10, *m/z* 379.20; I1:12, *m/z* 407.23; I2:20 (10,10), *m/z* 533.33; I3:22 (2,10,10), *m/z* 575.35, all with a mass window of 0.05 Da. All acylsugars are shown as formate adducts

2.4 | ASAT3H and ASAT4H produce triacylinositols that differ from the in vivo products

We performed in vitro assays to ask whether ASAT3H or ASAT4H have activities consistent with roles in acylinositol biosynthesis. We used a combined reaction containing *E. coli*-expressed His-tagged ASAT1H, ASAT4H, and ASAT3H with C2-CoA, nC10-CoA, and *myo*-inositol substrates. These acyl-CoA donors were used because those acyl chains are found in *S. quitoense* acylinositols. This assay produced an I3:22 (2,10,10) peak at pH 6 or 8 (Figures 4a and S14). MS fragmentation of the I3:22 (2,10,10) in vitro product matched the major *in planta* acylinositol (Figure S15), but the two compounds did not co-elute; this is consistent with acylation positions different from those of the in vivo metabolite (Figure 4b). The difference in in vitro and in vivo acylation positions suggests that *S. quitoense* acylinositol biosynthesis requires more than acylations of *myo*-inositol by the ASAT1H, ASAT3H, and ASAT4H enzymes.

The one pot combined reaction did not determine the relative order of action of ASAT4H and ASAT3H. To test the hypothesis that ASAT4H acetylates the I1:10 ASAT1H in vitro product, we combined ASAT1H and ASAT4H in a reaction with *myo*-inositol, C2-CoA and nC10-CoA at pH 6, yielding an I2:12 (2,10) product (Figures 4c and S16). Acetylation of I1:10 by ASAT4H was shown to occur with sequential assays containing C2-CoA, nC10-CoA, and *myo*-inositol with ASAT1H followed by heat inactivation and addition of ASAT4H, C2-CoA, and nC10-CoA yielded the I2:12 (2,10) product (Figure S17). In contrast, the reciprocal order—ASAT4H followed by ASAT1H—failed to yield I2:12 (2,10). These results indicate that ASAT1H acylates *myo*-inositol with nC10-CoA at Position R6, followed by acetylation by ASAT4H.

The cross-silencing of the other SlASAT4 homolog, SqTAIAT, by VIGS directed against ASAT4H (Figure S4) led us to ask whether it would also use $I1{:}10^{R6}$ as acyl acceptor. However, in contrast to ASAT4H, the combination of ASAT1H and TAIAT did not yield I2:12 (2,10) (Figure S18). Although the SqASAT4H acetyltransferase activity matches the other ASAT4 clade proteins Sl-ASAT4, SsASAT5, and TAIAT (Leong et al., 2020; Schilmiller et al., 2012), these other enzymes act on acceptor substrates that are tri- or tetra-acylated. ASAT4H is thus far unique in acetylating a monoacylated product in vitro (Fan et al., 2016; Leong et al., 2020; Moghe et al., 2017).

The results with a one pot assay containing three enzymes described above suggest that ASAT3H adds an nC10 acyl chain to I2:12 (2,10) to produce I3:22 (2,10,10). We used sequential assays to test this: Two enzymes were added together with C2-CoA, nC10-CoA and *myo*-inositol, followed by heat inactivation, and the addition of the third enzyme with more C2-CoA and nC10-CoA. The reaction with ASAT1H and ASAT4H followed by ASAT3H yielded both I2:12 (2,10) and I3:22 (2,10,10) consistent with ASAT3H catalyzing a third acylation (Figure S19). The reciprocal reaction with ASAT1H and ASAT3H followed by ASAT4H produced I2:12 (2,10) (presumably from consecutive reaction of ASAT1H and ASAT4H), but not I3:22 (2,10,10) (Figure S19). Taken together, these results indicate that ASAT3H can add an nC10 acyl chain to I2:12 (2,10) to make I3:22 (2,10,10), but does not acylate I1:10 to yield I2:20 (10,10). This is analogous to tomato acylsugar biosynthesis, where Sl-ASAT3 acylates diacylsucroses to yield triacylsucroses (Fan et al., 2016; Schilmiller et al., 2015).

2.5 | Conclusions

S. quitoense acylinositol biosynthesis is interesting due to the sugar core difference from previously characterized acylsugar pathways (Fan et al., 2016, 2017; Moghe et al., 2017; Nadakuduti et al., 2017). We hypothesized that acylinositol biosynthesis is evolutionarily related to acylsucrose biosynthesis in other Solanaceae species (Fan et al., 2016; Leong et al., 2020; Moghe et al., 2017). An *S. quitoense* TAIAT was previously shown to acetylate triacylinositols yielding tetraacylinositols (Leong et al., 2020). In this study, we describe characterization of three candidates (ASAT1H, ASAT4H, and ASAT3H) that are homologous to previously described ASATs (Figure 1) (Fan et al., 2016; Moghe et al., 2017; Schilmiller et al., 2012, 2015). These candidates were expressed and enriched in trichomes relative to shaved petiole tissue (Table 1) (Moghe et al., 2017). We used VIGS to test if these candidates are involved in *S. quitoense* acylinositol biosynthesis. VIGS results with both ASAT1H- and ASAT3H-targeted plants showed reduced total acylsugars consistent with an early step in acylinositol biosynthesis (Fan et al., 2016; Moghe et al., 2017; Nadakuduti et al., 2017). Silencing ASAT4H yields reduced total acylsugars and increased ratio of triacylinositols to tetraacylinositols. Interpreting the ASAT4H phenotype requires caution due to cross-silencing of TAIAT in the VIGS plants.

Results of in vitro biochemistry with these three candidates demonstrated ASAT-like activities with acceptor substrate specificities, but revealed products that are positional isomers of those detected from trichome extracts. ASAT1H catalyzes acylation of *myo*-inositol using nC10-CoA and nC12-CoA. It also possesses apparent K_m values similar to previously characterized ASATs. NMR analysis revealed that the acyl chain of the I1:10 product is not at a position on *myo*-inositol that matches the *in planta* acylsugars. In vitro assays revealed that the I1:10 product rearranges at pH 8, even in the absence of an enzyme. Assays with ASAT1H, ASAT4H, and ASAT3H showed an I3:22 (2,10,10) product that did not co-elute with the *in planta* I3:22 (2,10,10). Further in vitro assays indicated that ASAT1H acylated *myo*-inositol with an nC10-CoA first, followed by ASAT4H-catalyzed acetylation and then nC10 acyl chain addition by ASAT3H.

We propose several possibilities that could reconcile the conflict between the in vitro and *in planta* results. First, our in vitro experiments could be missing one or more enzymes involved in acylation at the positions observed *in planta*, for example, an acylsugar acyltransferase. This hypothesis could still include rearrangement at pH >6. Second, another class of enzyme—such as a serine carboxypeptidase-like enzyme (SCPL)—could play a role in acylinositol biosynthesis. SCPLs play roles in transferring acyl chains in other biosynthetic pathways (Mugford et al., 2009; Shirley et al., 2001; Stehle et al., 2008). Acylsugar hydrolases (*S. quitoense* transcripts

c33090_g1_i1/2 and c31412_g4_i1) are a third class of enzyme that could be involved in vivo: these remove acyl chains from acylsucroses and are trichome-enriched in *S. quitoense* (Moghe et al., 2017; Schilmiller et al., 2016). Perhaps edited acylsugars serve as substrates for other enzymes to generate the observed *in planta* product. Nonetheless, perturbation of the acylinositol phenotype due to VIGS of the BAHD enzymes strongly suggests that they are involved in acylinositol biosynthesis.

A third hypothesis is that *myo*-inositol is not the starting substrate for acylinositol biosynthesis. An analogous situation is seen in two *Solanum* species that make acylglucoses by acylating the disaccharide sucrose, followed by hydrolysis to acylglucose and fructose mediated by specialized invertases (Leong et al., 2019; Lou et al., 2021). In fact, *S. quitoense* accumulates acylated *myo*-inositol glycosides with sugar cores that could be the precursor of the *in planta* acylinositols (Hurney, 2018). *S. lanceolatum* is another species in the *Solanum* Leptostemonum clade that accumulates acylated inositol-glucose and inositol-xylose disaccharides (Herrera-Salgado et al., 2005). In the future, acylinositol accumulation in other *Solanum* species can be leveraged to understand how acylinositols are synthesized *in planta*.

Although it is disappointing that the in vitro products of ASAT1H, ASAT3H, and ASAT4H do not match the esterification positions of *S. quitoense* acylinositols characterized from trichome extracts, they can be employed for further studies. For example, the structurally-distinct in vitro-produced acylinositols are useful for testing the efficacy of different acylsugars on insects and pathogens. Protein structure and function analysis could reveal details about BAHD catalysis. In addition, the BAHD acyltransferases could be used to engineer acylinositol biosynthesis into other plants or microorganisms to search for biological activities.

3 | MATERIALS AND METHODS

3.1 | Candidate identification and phylogenetic characterization

Identification of suitable gene candidates was performed in our previous work (Leong et al., 2020). In short, sequences were selected based on the presence of the HXXXD motif (0 mismatches) and the DFGWG motif (1 mismatch allowed) using the "search for motif" function in Geneious R.8.1.9. Those sequences that qualified were filtered to those between 400 and 500 amino acids, and by relative position of the two motifs (DAuria, 2006). Eggplant putative ASAT homologs were obtained by blasting Sl-ASAT1-4 and Solyc07g043670 coding sequence against the Eggplant genome v3 CDS sequences on Sol Genomics Network using blastn.

Sequences were aligned against other characterized BAHD sequences and characterized ASATs using MEGA X (Kumar et al., 2018). The evolutionary history was inferred by using the maximum likelihood method and Whelan and Goldman + Freq. model (Whelan & Goldman, 2001). The bootstrap consensus tree inferred from 1000 replicates (Felsenstein, 1985) is taken to represent the evolutionary history of the taxa analyzed (Felsenstein, 1985). Branches corresponding to partitions reproduced in less than 50% bootstrap replicates are collapsed. Initial tree(s) for the heuristic search were obtained automatically by applying Neighbor-Join and BioNJ algorithms to a matrix of pairwise distances estimated using the JTT model, and then selecting the topology with superior log likelihood value. A discrete Gamma distribution was used to model evolutionary rate differences among sites (5 categories [+G, parameter = 1.9258]). This analysis involved 63 amino acid sequences. All positions with less than 30% site coverage were eliminated, that is, fewer than 70% alignment gaps, missing data, and ambiguous bases were allowed at any position (partial deletion option). There were a total of 459 positions in the final dataset.

3.2 | Heterologous protein expression and purification from *Escherichia coli*

Heterologous protein expression was achieved using pET28b(+) (EMD Millipore, Burlington, MA, USA), in which open reading frames for the enzymes were cloned into using doubly digested vectors of either BamHI/XhoI (ASAT4H), NheI/XhoI (ASAT1H), or NheI/NotI (c8981_g1_i1). The doubly digested vectors were assembled with a single fragment containing the ORF containing 5′ and 3′ adapters for Gibson assembly using 2× NEB Hifi Mastermix (NEB, Ipswich, MA, USA). The finished constructs were transformed into BL21 Rosetta (DE3) cells (EMD Millipore, Burlington, MA, USA) and verified using colony PCR and Sanger sequenced using T7 promoter and terminator primers. Oligonucleotide sequences are presented in Table S7.

LB overnight cultures with kanamycin (50 μg/ml) and chloramphenicol (33 μg/ml) were inoculated with a single colony of the bacterial strain containing the desired construct and incubated at 37°C, 225 rpm, overnight. Larger cultures were inoculated 500:1 with the same antibiotics and incubated at the same temperature and speed. OD600 of the cultures was monitored until between 0.5 and 0.8. Cultures were chilled on ice for 15 min, at which IPTG was added to a final concentration of 50 μM for all BAHD sequences except for ASAT1H, which was incubated with 300-μM IPTG. Cultures were incubated at 16°C, 180 rpm for 16 h.

Note: all of the following steps were processed on ice.

Cultures were centrifuged at 4000 *g* for 10 min to collect the cells and repeated until all the culture was processed (4°C). The cell pellets were resuspended in 25 ml of extraction buffer (50-mM $NaPO_4$, 300-mM NaCl, 20-mM imidazole, 5-mM 2-mercaptoethanol, pH 8.0) by vortexing. The cell suspension was sonicated for eight cycles (30 s on, intensity 4, 30 s on ice). The cellular extracts were centrifuged at 30,000 *g* for 10 min. The supernatant was transferred into another tube and centrifuged again at the same speed and duration. Ni-NTA resin (Qiagen, Hilden, Germany) was centrifuged at 1000 *g* for 1 min, resuspended in 1 ml of extraction buffer. The slurry was centrifuged again at 1000 *g* for 1 min and the supernatant was decanted. The resin was resuspended using the crude extract and incubated at 4°C, nutating for 1 h. The slurry was centrifuged at

3200 *g* for 5 min, and supernatant decanted. The resin was resuspended in 5 ml of extraction buffer and transferred to a gravity flow column (Bio Rad, Hercules, CA, USA). After loading, the resin was washed with three column volumes of extraction buffer (~30 ml). The resin was further washed with one column volume of wash buffer (extraction buffer with 40-mM imidazole). The remaining protein was eluted and collected using 2 ml of elution buffer after a 1-min incubation with the resin. The elution was diluted into 15 ml of storage buffer (extraction buffer, but no imidazole). This elution was concentrated using 30-kDa centrifugal filter units (EMD Millipore, Burlington, MA, USA), and repeated until diluted 1000-fold. An equal volume of 80% glycerol was added to the elution, mixed, and stored at −20°C.

3.3 | General enzyme assays

Assays were run in 100-mM sodium phosphate, pH 6, or pH 8 at a total volume of 60 µl with pH 6 as the default unless otherwise stated. Acyl-CoAs were added to a final concentration of 100 µM. Non-acylated acceptors were added at a final concentration of 1 mM. 6 µl of enzyme was added to each reaction. The assays were incubated at 30°C for 30 min unless otherwise stated. After the incubation, two volumes of stop solution—composed of 1:1 (v/v) of acetonitrile and isopropanol with 0.1% formic acid and 1-µM telmisartan as internal standard (Sigma-Aldrich, St. Louis, MO, USA)—were added to the assays and mixed by pipetting. Reactions were stored in the −20°C freezer for 20 min and centrifuged at 17,000 *g* for 5 min. The supernatant was transferred to LC–MS tubes and stored at −20°C.

ASAT1H time-point assays at pH 8 were scaled up to 200-µl reactions with the same proportions of reagents to allow time-point aliquots. Assays that tested ASAT1H and ASAT4H together were run with 50-mM *myo*-inositol, 3 µl of each enzyme was added to each 60-µl reaction, and incubated for 30 min, unless otherwise stated. Sequential assays testing ASAT1H or 4H order included an initial incubation of 30°C for 30 min with the first enzyme (volume is 60 µl at this point), a 70°C incubation for 10 min to inactivate the enzyme, followed by addition of 3 µl each of 2-mM decanoyl-CoA, acetyl-CoA, and 3 µl of the second enzyme with a 30-minincubation at 30°C. Joint assays with ASAT1, 3, and 4H together included 2 µl of each enzyme, 50-mM *myo*-inositol, and were incubated for 2 h. Sequential assays testing ASAT1H, 3H, and 4H included a similar format: 2 µl of ASAT1H and ASAT3 or 4H (60-µl total volume) with a 1-h incubation at 30°C, assays were incubated at 70°C for 10 min to inactivate enzymes, followed by the addition of 2 µl of the last enzyme and 3 µl each of 2-mM decanoyl and acetyl-CoA and a 1-h incubation at 30°C.

For kinetic analysis, conditions were used such that the enzyme amount and reaction time were in the linear range. For each substrate (nC10, nC12, and *myo*-inositol), the other substrate was held at saturating concentrations. The reactions were run for 20 min, performed in triplicate, and stopped by the addition of 2 volumes of stop solution. Samples were analyzed as described in section 3.6. Nonlinear regression was performed using standard Michaelis–Menten kinetics model in GraphPad Prism 8 (GraphPad software).

For rearrangement assays, a 10-ml reaction with 1 ml of ASAT1H in 100-mM sodium phosphate, pH 6 with 100-µM decanoyl-CoA and 75-mM *myo*-inositol was run for 3 h. Reactions were stopped with two volumes of stop solution (1:1 acetonitrile:isopropanol with 0.1% formic acid), dried down by SpeedVac and resuspended in 8 ml of water:acetonitrile (6:4) and purified by method for the single-product NMR analysis in NMR analysis of monoacylinositols below except that the purified fraction was resuspended in 2 ml of water: acetonitrile with 0.1% formic acid and dried down before storage at −20°C. Assays were run in 100-mM sodium phosphate, pH 6 and 8. I1:10 product was resuspended in an ethanol:water mixture (1:1), and 1/60th of a volume was added to the reaction. Time-point assays were run and sampled at 5, 10, 15, 30, 45, and 60 min. Serial dilutions of monoacylinositol products confirmed that proportions of isomers are maintained by LC–MS (Figure S10, Tables S5 and S6).

3.4 | Mono-acylated enzyme assays for NMR analysis

Assays for single-product NMR analyses were run in 100-mM ammonium acetate, pH 6.0 at a total volume of 60 ml. nC10-CoA and *myo*-inositol were added to a final concentration of 400 µM and 30 mM, respectively. A 6-mL of enzyme solution was added to the reactions purified from 6 L of *E. coli* culture. Reactions were incubated at 30°C for 3 h. After incubation, two volumes of stop solution—1:1 acetonitrile: isopropanol containing 0.1% formic acid—were added to the assays and mixed by pipetting. The multiproduct NMR analysis was similar except it was run in 50-mM ammonium acetate, pH 6 with 100-µM nC10-CoA and 75-mM *myo*-inositol, and incubated at 30°C for 45 min. Reactions were evaporated to dryness using the SpeedVac. In both cases, the products were purified using a Waters 2795 Separations module equipped with LKB Bromma 2211 Superrac fraction collector with automated fraction collection.

3.5 | Purification and NMR analysis of monoacylinositols

For the single mono-acylated NMR product analysis, the residue was resuspended in a 6-ml mixture of water and acetonitrile (6:4) with 0.1% formic acid by vortexing and transferred to LC–MS vials for semipreparative purification. Samples were purified on the semi-preparative LC using 200-µl injections at a flow rate of 1.5 ml/min using a C18 semipreparative column at 30°C (Acclaim C18 5 µm 120 Å, 4.6 × 150 mm, Thermo Fisher). Solvents A and B were water with 0.1% formic acid and acetonitrile, respectively. The 24-minlinear LC gradient was as follows: 5% B at 0 min; 25% B at 1.00 min; 35% B at 20.00 min; 100% B at 21.00 min; 100% B until 22.00 min; 5% B at 22.01 min; 5% B until 24.00 min. The duration of collection of each fraction was 15 s. The 14-min I1:10 method described in Section 3

was used to analyze fractions using mass spectrometry. Fraction 72 was evaporated to dryness in a SpeedVac. The residue was resuspended in a 1-ml mixture of water:acetonitrile (6:4) with 0.1% formic acid. The solution was dried in a SpeedVac and resuspended in deuterated acetonitrile before being transferred to Shigemi tubes for NMR analysis. ^{1}H, ^{13}C, gCOSY, gHSQC, gHMBC, and NOESY NMR experiments were performed at the Max T. Rogers NMR Facility at Michigan State University using a Bruker Avance 900 spectrometer equipped with a TCI triple resonance probe. All spectra were referenced to non-deuterated CD_3CN solvent signals ($\delta_H = 1.94$ and $\delta_C = 1.32$, 118.26 ppm). The ^{1}H spectra were recorded at 900 MHz, while the ^{13}C spectra were recorded at 225 MHz.

For the NMR sample containing multiple monoacylinositol isomers, the dried acylsugar was resuspended in a 6-ml mixture of water and acetonitrile (6:4) with 0.1% formic acid by vortexing and the solvent was evaporated under vacuum using a Thermo Savant SPD 131 DDA SpeedVac concentrator with BOC Edwards XDS scroll pump. The residue was reconstituted in acetonitrile:isopropanol (ACN:IPA) (1:1) with sonication, combined to a single 18 × 150 mm tube and concentrated to dryness under vacuum using the SpeedVac. Approximately 300 μl of ACN:IPA (1:1) was added to the tube, sonicated, and centrifuged. The supernatant was then transferred to an LC autosampler vial with limited volume insert for semi-preparative high-performance liquid chromatography (HPLC) purification (~250-μl sample volume). The purification was performed by semipreparative LC via two 200-μl injections using a C18 semipreparative column at 50°C (Acclaim C18 5 μm 120 Å, 4.6 × 150 mm). To maximize sample recovery, after the first injection, approximately 150 μl of AcN:IPA was added to the culture tube, sonicated and centrifuged. The supernatant was then transferred to the same LC autosampler vial with limited volume insert for a second injection.

One-minute fractions were collected in Pyrex glass culture tubes (18 × 150 mm, total volume 3 ml each fraction) and labeled by minute. The 50-min LC gradient had Solvents A, 0.15% formic acid in water; B, acetonitrile; and column wash with C, dichloromethane:acetone:methanol (v/v/v, 1;1:1). The linear gradient began with a hold at 5% B from 0 to 1 min, ramp from 5% to 20% B from 1 to 2 min, ramp from 20% to 40% B from 2 to 25 min The fractions were combined according to the observed purity and the abundance of the ion at *m/z* 379.20, consistent with $[M + HCOO]^-$ of C10 monoacylinositols. Fractions 16–21 had the greatest abundance. Those fractions were combined and concentrated to dryness under vacuum for NMR, and ramp from 40% to 100% B from 25 to 26 min. The solvent profile continued with a hold at 100% B from 26 to 28 min, ramp from 100% B to 100% C from 28 to 29 min, hold at 100% C from 29 to 39 min, and ramp from 100% C to 100% B from 39 to 40 min. The final stages of the solvent gradient were a ramp from 100% to 5% B from 40% to 41 min, and hold at 5% B for 41 to 50 min. The sample was dissolved in ~250-μl acetonitrile-d_3 with vortex mixing and transferred to a solvent matched Shigemi tube and analyzed by ^{1}H-NMR. The NMR spectrum was recorded using a Bruker Avance 900-MHz NMR spectrometer equipped with a TCI triple-resonance inverse detection cryoprobe at the Max T. Rogers NMR facility at Michigan State University.

For the LC–MS analysis of monoacylinositol isomers (Figure S10), the following LC gradient used Solvents A, 10-mM ammonium formate, pH 2.8 in water; and B, acetonitrile. Samples were analyzed on a Waters Acquity ultra-performance liquid chromatography (UPLC) coupled to a Waters Xevo G2-XS QToF mass spectrometer with an Acquity UPLC HSS-T3 C18 column (2.1 mm × 100 mm × 1.8 μm). The gradient with a flow rate of 0.5 ml/min is as follows: Hold at 99% A from 0 to 1 min, ramp to 50% A from 1 to 5 min, ramp to 100% A from 10 to 10.01 min, hold at 100% A from 10.01 to 12.50 min, ramp to 99% A from 12.50 to 12.51 min, and hold at 99% A from 12.51 to 15.00 min.

3.6 | LC–MS analysis

LC–MS samples (both enzyme assays and plant samples) were analyzed on a Waters Acquity UPLC coupled to a Waters Xevo G2-XS QToF mass spectrometer (Waters Corporation, Milford, MA, USA). Sample injection volume was 10 μl. LC–MS methods were performed with gradient elution using an Ascentis Express C18 HPLC column (10 cm × 2.1 mm, 2.7 μm) (Sigma-Aldrich, St. Louis, MO, USA) at 40°C using the following solvents: 10-mM ammonium formate, pH 2.8 as Solvent A, and 100% acetonitrile as Solvent B. A flow rate of 0.3 ml/min was used unless otherwise specified. All LC–MS was performed with electrospray ionization in either positive or negative ion mode as described.

A 7-min linear elution gradient consisted of 5% B at 0 min, 60% B at 1 min, 100% B at 5 min, held at 100% B until 6 min, 5% B at 6.01 min and held at 5% until 7 min.

A 14 min, I1:10 linear elution gradient consisted of 5% B at 0 min; 25% B at 1 min; 50% B at 10 min; 100% B at 12 min; 5% B at 12.01 min, 5% B at 14.00 min. This method is the default 14-min method unless otherwise stated.

An alternative 14-min linear elution gradient was used for the comparison of I3:22 metabolites extracted from *S. quitoense* or generated in an enzyme assay containing ASAT1H and TAIAT or ASAT4H. The 14-min linear elution gradient consisted of 5% B at 0 min; 60% B at 1 min; 100% B at 12 min; 100% B at 13 min; 5% B at 13.01 min, 5% B at 14.00 min.

A 21-min linear elution gradient of 5% B at 0 min, 60% B at 3 min, 100% B at 15 min, held at 100% B until 18 min, 5% B at 18.01 min and held at 5% until 21 min.

For electrospray ionization (ESI)-MS settings, the following were used: capillary voltage, 2.00 kV; source temperature, 100°C; desolvation temperature, 350°C; desolvation nitrogen gas flow rate, 600 L/h; cone voltage, 40 V; mass range, *m/z* 50–1000 (with spectra accumulated at 0.1 s per function). Three quasi-simultaneous acquisition functions were used to acquire spectra at different collision potentials (0, 15, and 35 V). Lock mass correction was performed using leucine enkephalin as the reference for data acquisition.

For ESI + MS settings, the following were used: capillary voltage, 3.00 kV; source temperature, 100°C; desolvation temperature, 350°C; desolvation nitrogen gas flow rate, 600 L/h; cone voltage, 35 V; mass range, *m/z* 50–1000 (with spectra accumulated at 0.1 s per function). Two acquisition functions were used to acquire spectra at different collision potential settings (0, 10–60 V). Lock mass correction was performed using leucine enkephalin as the reference for data acquisition.

LC–MS/MS analyses were performed using the same instruments and columns as the other LC–MS analysis. Ion source parameters were as described above. Survey scans were acquired over *m/z* 50 to 1000 with 0.3 s per scan. Collision potential was ramped from 10–60 V. For I2:12, the formate adduct (*m/z* 421.20) was used. For I3:22, the ammonium adduct (*m/z* 548.38) and formate adduct (*m/z* 575.34) were used for analysis.

For K_m measurements, the same column, 7-min LC method, and solvents were used for the analysis on the Waters Acquity TQD triple quadrupole mass spectrometer coupled to a Waters Acquity UPLC. The parameters used for the mass spectrometer are as follows: capillary voltage, 2.5 kV; cone voltage, 30 V; source temperature, 130°C; desolvation temperature, 350°C; cone gas flow, 20 L/h; desolvation gas flow, 800 L/h. The mass pairs used are as follows: telmisartan, *m/z* 513 > 287; I1:10, *m/z* 379 > 171; *m/z* I1:12, 407 > 199.

3.7 | VIGS analysis

pTRV2-LIC was digested using PstI-HF to generate the linearized vector. The linearized vector was purified using a 1% agarose gel and gel extracted using an Omega EZNA gel extraction kit. Fragments were amplified using PCR with adapters for ligation into pTRV2-LIC. Both the PCR fragment and the linearized vector were incubated in separate 5-μl reactions using NEB 2.1 as buffer with T4 DNA polymerase and 5-mM dATP or dTTP (PCR insert/Vector). The reactions were incubated at 22°C for 30 min, subsequently incubated at 70°C for 20 min. The reactions were then stored on ice. A 1 μl of the pTRV2-LIC reaction and 2 μl of the PCR-LIC reaction were mixed by pipetting. Reactions were incubated at 65°C for 2 min, then 22°C for 10 min. After which the constructs were transformed into chemically competent *E. coli* cells.

Constructs were tested for the presence of the insert using colony PCR and pTRV2-LIC-seq-F/R primers showing a 300-bp insertion. Positive constructs were miniprepped (Qiagen, Hilden, Germany) and Sanger sequenced using the same primers. Sequenced constructs and pTRV1 were transformed into agrobacterium strain, GV3101, using the protocol described previously except on LB plates with kanamycin (50 μg/ml), rifampicin (50 μg/ml), and gentamycin (10 μg/ml). Colonies were assayed for the presence of the insert using the colony PCR and the pTRV2-LIC-seq-F/R primers previously described. The presence of the pTRV1 vector in GV3101 was assayed using colony PCR primers, pTRV1-F/R.

The protocol was adapted from Velásquez et al. (2009). Seeds were germinated using incubation in 10% bleach for 30 min, followed by five to six washes with water. Seeds were transferred to a petri dish with Whatman paper and water in the bottom of the dish. Seeds were stored in a lab drawer until hypocotyls emerge, at which point they were moved to a window sill. Once cotyledons had emerged, seedlings were transferred to peat pots and grown for approximately 1 week under 16/8 day/night cycle at 24°C. At 2 days pre-inoculation, LB cultures (Kan/Rif/Gent) were inoculated with the cultures used for leaf inoculation. The strains had constructs containing the gene of interest (GOI) in pTRV2-LIC, an empty vector pTRV2-LIC, and pTRV1. Cultures were grown overnight at 30°C with shaking at 225 rpm. Larger cultures composed of induction media (4.88-g MES, 2.5-g glucose, 0.12-g sodium phosphate monobasic monohydrate in 500 ml, pH 5.6, 200-μM acetosyringone), were inoculated using a 25:1 dilution of the overnight culture (50-ml total). The larger culture was incubated at 30°C, 225 rpm, overnight. Cells were harvested by centrifugation at 3200 *g* for 10 min. Cell pellets were resuspended in 1 volume of 10-mM MES, pH 5.6, 10-mM $MgCl_2$. Cells were gently vortexed to resuspend the pellet. Cell suspensions were centrifuged at 3200 *g* for 10 min. Cell pellets were resuspended in 10-ml of 10-mM MES, pH 5.6, 10-mM $MgCl_2$. The OD600 values were measured for each of the cultures. Cell suspensions were diluted using the same buffer to an OD600 of 1. Acetosyringone was added to the pTRV1 cell suspension to a final concentration of 400 μM. The different pTRV2-LIC constructs were mixed into 50-ml conical tubes with an equal volume of pTRV1 suspension, resulting in a final acetosyringone concentration of 200 μM. Individual seedlings were inoculated through the abaxial side of the cotyledon. Plants were incubated at 22°C and shaded for 24 h. After 24 h, the plants were returned to 16/8 h day/night cycles at the same temperature. Approximately 3 weeks later, the plants were sampled for acylsugars and RNA using a bisected leaf for each experiment. Note that inoculation timing is very important; the cotyledons should be inoculated after they have expanded, but before the first two true leaves have fully emerged.

3.8 | Acylsugar analysis

The interactive protocol for acylsugar extracts is available at Protocols.io online (https://doi.org/10.17504/protocols.io.xj2fkqe).

The acylsugar extraction protocol was described in (Leong et al., 2019). LC–MS conditions used for acylsugar analysis were described the Section 3.6.

3.9 | qRT-PCR analysis

RNA was extracted with the RNeasy Plant Mini Kit including on-column DNase digestion (Qiagen), according to the manufacturer's instructions. RNA was quantified with a NanoDrop 2000c instrument (Thermo Fisher Scientific). cDNA was synthesized using 1 mg of the isolated RNA and SuperScript II Reverse Transcriptase (Invitrogen). The cDNA samples were diluted 20-fold (10-fold initial dilution and

2-fold dilution before quantitative polymerase chain reactions [qPCRs]). qPCRs (10 ul) were created with SYBR Green PCR Master Mix with 1 µl of cDNA added (Thermo Fisher Scientific). Primers were used at a final concentration of 200 nM. RT_ASAT1H_F/R, RT_ASAT3H_F/R, RT_ASAT4H_F/R, RT_TAIAT_F/R,RT_Actin_F/R, and RT_EF1a_F/R primers were used to detect ASAT1H, ASAT3H, ASAT4H, TAIAT, ACTIN, and EF1a transcripts, respectively (Table S7). Reactions were carried out with a QuantStudio 7 Flex Real-Time PCR System (Applied Bio-systems) by the Michigan State University RTSF Genomics Core. The following temperature cycling conditions were applied: 50°C for 2 min, 95°C for 10 min, and 40 cycles of 95°C for 15 s and 60°C for 1 min. Relative expressions of ASAT1H, ASAT3H, ASAT4H, and TAIAT were calculated with the DDCt method (Pfaffl, 2001) and normalized to the geometric mean of ACTIN and EF1a transcript levels. The mean expression values of the transcripts in the control plants were used for normalization. Three to four technical replicates were used for all the qPCRs.

3.10 | Accession numbers

ASAT homolog sequence data are available in GenBank as follows: TAIAT, MT024677; c38687_g1_i1, MT024678; c38687_g2_i1, MT024679; c39979_g2_i1, ON005014; c8981_g1_i1, ON005015.

AUTHOR CONTRIBUTIONS

All authors designed the original research; Bryan J. Leong, Steven M. Hurney, Thilani M. Anthony, and Paul D. Fiesel. performed the experiments; Bryan J. Leong, Steven M. Hurney., and Robert L. Last wrote the manuscript; all authors edited the article.

FUNDING INFORMATION

This research was funded by the National Science Foundation grant IOS-PGRP-1546617 (to R. L. L. and A. D. J.) and National Institute of General Medical Sciences of the National Institutes of Health graduate training grant no. T32-GM110523 (to B. J. L. and P. D. F.). A. D. J. is supported in part by USDA National Institute of Food and Agriculture Hatch project number MICL02474.

CONFLICT OF INTEREST

The Authors did not report any conflict of interest.

DATA AVAILABILITY STATEMENT

Datasets and materials used in this study available upon reasonable request.

ORCID

Bryan J. Leong https://orcid.org/0000-0003-4042-1160
Steven Hurney https://orcid.org/0000-0001-8490-7213
Paul Fiesel https://orcid.org/0000-0002-2038-5417
Gaurav Moghe https://orcid.org/0000-0002-8761-064X
Arthur Daniel Jones https://orcid.org/0000-0002-7408-6690
Robert L. Last https://orcid.org/0000-0001-6974-9587

REFERENCES

Ahuja, I., Kissen, R., & Bones, A. M. (2012). Phytoalexins in defense against pathogens. *Trends in Plant Science*, *17*, 73–90. https://doi.org/10.1016/j.tplants.2011.11.002

Burke, B., Goldsby, G., & Mudd, J. B. (1987). Polar epicuticular lipids of *Lycopersicon pennellii*. *Phytochemistry*, *26*(9), 2567–2571. https://doi.org/10.1016/S0031-9422(00)83879-0

DAuria, J. C. (2006). Acyltransferases in plants: A good time to be BAHD. *Current Opinion in Plant Biology*, *9*, 331–340. https://doi.org/10.1016/j.pbi.2006.03.016

Fan, P., Leong, B. J., & Last, R. L. (2019). Tip of the trichome: Evolution of acylsugar metabolic diversity in Solanaceae. *Current Opinion in Plant Biology*, *49*, 8–16. https://doi.org/10.1016/j.pbi.2019.03.005

Fan, P., Miller, A. M., Liu, X., Jones, A. D., & Last, R. L. (2017). Evolution of a flipped pathway creates metabolic innovation in tomato trichomes through BAHD enzyme promiscuity. *Nature Communications*, *8*(1), 2080. https://doi.org/10.1038/s41467-017-02045-7

Fan, P., Miller, A. M., Schilmiller, A. L., Liu, X., Ofner, I., Jones, A. D., Zamir, D., & Last, R. L. (2016). *In vitro* reconstruction and analysis of evolutionary variation of the tomato acylsucrose metabolic network. *Proceedings of the National Academy of Sciences*, *113*, E239–E248. https://doi.org/10.1073/pnas.1517930113

Fan, P., Wang, P., Lou, Y.-R., Leong, B. J., Moore, B. M., Schenck, C. A., Combs, R., Cao, P., Brandizzi, F., Shiu, S.-H., & Last, R. L. (2020). Evolution of a plant gene cluster in Solanaceae and emergence of metabolic diversity. *eLife*, *9*, e56717. https://doi.org/10.7554/eLife.56717

Felsenstein, J. (1985). Confidence limits on phylogenies: An approach using the bootstrap. *Evolution*, *39*(4), 783–791. https://doi.org/10.1111/j.1558-5646.1985.tb00420.x

Ghosh, B., Westbrook, T. C., & Jones, A. D. (2014). Comparative structural profiling of trichome specialized metabolites in tomato (*Solanum lycopersicum*) and *S. habrochaites*: Acylsugar profiles revealed by UHPLC/MS and NMR. *Metabolomics*, *10*(3), 496–507. https://doi.org/10.1007/s11306-013-0585-y

Herrera-Salgado, Y., Garduño-Ramírez, M. L., Vázquez, L., Rios, M. Y., & Alvarez, L. (2005). *Myo*-inositol-derived glycolipids with anti-inflammatory activity from *Solanum lanceolatum*. *Journal of Natural Products*, *68*(7), 1031–1036. https://doi.org/10.1021/np050054s

Howe, G. A., & Jander, G. (2008). Plant immunity to insect herbivores. *Annual Review of Plant Biology*, *59*(1), 41–66. https://doi.org/10.1146/annurev.arplant.59.032607.092825

Hurney, S. M. (2018). Strategies for profiling and discovery of acylsugar specialized metabolites. [Doctoral dissertation, Michigan State University]. Proquest.

Kim, J., Kang, K., Gonzales-Vigil, E., Shi, F., Jones, A. D., Barry, C. S., & Last, R. L. (2012). Striking natural diversity in glandular trichome acylsugar composition is shaped by variation at the Acyltransferase2 locus in the wild tomato *Solanum habrochaites*. *Plant Physiology*, *160*(4), 1854–1870. https://doi.org/10.1104/pp.112.204735

King, R. R., & Calhoun, L. A. (1988). 6 2,3-Di-O- and 1,2,3-tri-O-acylated glucose esters from the glandular trichomes of Datura metel. *Phytochemistry*, *27*(12), 3761–3763. https://doi.org/10.1016/0031-9422(88)83013-9

King, R. R., Pelletier, Y., Singh, R. P., & Calhoun, L. A. (1986). 3,4-Di-*O*-isobutyryl-6-O-caprylsucrose: The major component of a novel sucrose ester complex from the type B glandular trichomes of *Solanum berthaultii* hawkes (PI 473340). *Journal of the Chemical Society, Chemical Communications*, *14*, 1078–1079. https://doi.org/10.1039/c39860001078

Kumar, S., Stecher, G., Li, M., Knyaz, C., & Tamura, K. (2018). MEGA X: Molecular evolutionary genetics analysis across computing platforms. *Molecular Biology and Evolution*, *35*(6), 1547–1549. https://doi.org/10.1093/molbev/msy096

Landis, J. B., Miller, C. M., Broz, A. K., Bennett, A. A., Carrasquilla-Garcia, N., Cook, D. R., Last, R. L., Bedinger, P. A., & Moghe, G. D. (2021). Migration through a major Andean ecogeographic disruption as a driver of genetic and phenotypic diversity in a wild tomato species. *Molecular Biology and Evolution*, *38*(8), 3202–3219. https://doi.org/10.1093/molbev/msab092

Landry, L. G., Chapple, C. C. S., & Last, R. L. (1995). Arabidopsis mutants lacking phenolic sunscreens exhibit enhanced ultraviolet-B injury and oxidative damage. *Plant Physiology*, *109*(4), 1159–1166. https://doi.org/10.1104/pp.109.4.1159

Leong, B. J. (2019). Analysis of acylglucose and acylinositol biosynthetic mechanisms in Solanaceae species. [Doctoral dissertation, Michigan State University]. Proquest.

Leong, B. J., Hurney, S. M., Fiesel, P. D., Moghe, G. D., Jones, A. D., & Last, R. L. (2020). Specialized metabolism in a nonmodel nightshade: Trichome acylinositol biosynthesis. *Plant Physiology*, *183*(3), 915–924. https://doi.org/10.1104/pp.20.00276

Leong, B. J., Lybrand, D. B., Lou, Y.-R., Fan, P., Schilmiller, A. L., & Last, R. L. (2019). Evolution of metabolic novelty: A trichome-expressed invertase creates specialized metabolic diversity in wild tomato. *Science Advances*, *5*(4), eaaw3754. https://doi.org/10.1126/sciadv.aaw3754

Liu, X., Enright, M., Barry, C. S., & Jones, A. D. (2017). Profiling, isolation and structure elucidation of specialized acylsucrose metabolites accumulating in trichomes of *Petunia* species. *Metabolomics*, *13*(7), 85. https://doi.org/10.1007/s11306-017-1224-9

Lou, Y.-R., Anthony, T. M., Fiesel, P. D., Arking, R. E., Christensen, E. M., Jones, A. D., & Last, R. L. (2021). It happened again: Convergent evolution of acylglucose specialized metabolism in black nightshade and wild tomato. *Science Advances*, *7*, eabj8726. https://doi.org/10.1126/sciadv.abj8726

Lybrand, D. B., Anthony, T. M., Jones, A. D., & Last, R. L. (2020). An integrated analytical approach reveals trichome acylsugar metabolite diversity in the wild tomato *Solanum pennellii*. *Metabolites*, *10*, 1–25. https://doi.org/10.3390/metabo10100401

Maldonado, E., Torres, F. R., Martínez, M., & Pérez-Castorena, A. L. (2006). Sucrose esters from the fruits of *Physalis nicandroides* var. attenuata. *Journal of Natural Products*, *69*(10), 1511–1513. https://doi.org/10.1021/np060274l

Mandal, S., Ji, W., & McKnight, T. D. (2020). Candidate gene networks for acylsugar metabolism and plant defense in wild tomato *Solanum pennellii*. *The Plant Cell*, *32*(1), 81–99. https://doi.org/10.1105/tpc.19.00552

Massalha, H., Korenblum, E., Tholl, D., & Aharoni, A. (2017). Small molecules below-ground: The role of specialized metabolites in the rhizosphere. *Plant Journal*, *90*(4), 788–807. https://doi.org/10.1111/tpj.13543

Matsuzaki, T., Shinozaki, Y., Suhara, S., Shigematsu, H., & Koiwai, A. (1989). Isolation and characterization of tetra- and triacylglucose from the surface lipids of *Nicotiana miersii*. *Agricultural and Biological Chemistry*, *53*(12), 3343–3345. https://doi.org/10.1271/bbb1961.53.3343

Mithöfer, A., & Boland, W. (2012). Plant defense against herbivores: Chemical aspects. *Annual Review of Plant Biology*, *63*(1), 431–450. https://doi.org/10.1146/annurev-arplant-042110-103854

Moghe, G. D., Leong, B. J., Hurney, S., Daniel Jones, A., & Last, R. L. (2017). Evolutionary routes to biochemical innovation revealed by integrative analysis of a plant-defense related specialized metabolic pathway. *eLife*, *6*, 1–33. https://doi.org/10.7554/eLife.28468

Mugford, S. T., Qi, X., Bakht, S., Hill, L., Wegel, E., Hughes, R. K., Papadopoulou, K., Melton, R., Philo, M., Sainsbury, F., Lomonossoff, G. P., Roy, A. D., Goss, R. J. M., & Osbourn, A. (2009). A serine carboxypeptidase-like acyltransferase is required for synthesis of antimicrobial compounds and disease resistance in oats. *The Plant Cell*, *21*(8), 2473–2484. https://doi.org/10.1105/tpc.109.065870

Nadakuduti, S. S., Uebler, J. B., Liu, X., Jones, A. D., & Barry, C. S. (2017). Characterization of trichome-expressed BAHD acyltransferases in *Petunia axillaris* reveals distinct acylsugar assembly mechanisms within the Solanaceae. *Plant Physiology*, *175*, 36–50. https://doi.org/10.1104/pp.17.00538

Ning, J., Moghe, G. D., Leong, B. J., Kim, J., Ofner, I., Wang, Z., Adams, C., Jones, A. D., Zamir, D., & Last, R. L. (2015). A feedback-insensitive isopropylmalate synthase affects acylsugar composition in cultivated and wild tomato. *Plant Physiology*, *169*, 1821–1835. https://doi.org/10.1104/pp.15.00474

Schilmiller, A. L., Charbonneau, A. L., & Last, R. L. (2012). Identification of a BAHD acetyltransferase that produces protective acyl sugars in tomato trichomes. *Proceedings of the National Academy of Sciences*, *109*(40), 16377–16382. https://doi.org/10.1073/pnas.1207906109

Schilmiller, A. L., Gilgallon, K., Ghosh, B., Jones, A. D., & Last, R. L. (2016). Acylsugar acylhydrolases: Carboxylesterase catalyzed hydrolysis of acylsugars in tomato trichomes. *Plant Physiology*, *170*(3), 1331–1344. https://doi.org/10.1104/pp.15.01348

Schilmiller, A. L., Moghe, G. D., Fan, P., Ghosh, B., Ning, J., Jones, A. D., & Last, R. L. (2015). Functionally divergent alleles and duplicated loci encoding an acyltransferase contribute to acylsugar metabolite diversity in *Solanum* trichomes. *The Plant Cell*, *27*(4), 1002–1017. https://doi.org/10.1105/tpc.15.00087

Shirley, A. M., McMichael, C. M., & Chapple, C. (2001). The *sng2* mutant of *Arabidopsis* is defective in the gene encoding the serine carboxypeptidase-like protein sinapoylglucose: Choline sinapoyltransferase. *Plant Journal*, *28*(1), 83–94. https://doi.org/10.1046/j.1365-313X.2001.01123.x

Stehle, F., Brandt, W., Schmidt, J., Milkowski, C., & Strack, D. (2008). Activities of Arabidopsis sinapoylglucose: Malate sinapoyltransferase shed light on functional diversification of serine carboxypeptidase-like acyltransferases. *Phytochemistry*, *69*(9), 1826–1831. https://doi.org/10.1016/j.phytochem.2008.03.021

Stevenson, P. C., Nicolson, S. W., & Wright, G. A. (2017). Plant secondary metabolites in nectar: Impacts on pollinators and ecological functions. *Functional Ecology*, *31*(1), 65–75. https://doi.org/10.1111/1365-2435.12761

Velásquez, A. C., Chakravarthy, S., & Martin, G. B. (2009). Virus-induced gene silencing (VIGS) in *Nicotiana benthamiana* and tomato. *JoVE*, *28*, e1292.

Whelan, S., & Goldman, N. (2001). A general empirical model of protein evolution derived from multiple protein families using a maximum-likelihood approach. *Molecular Biology and Evolution*, *18*(5), 691–699. https://doi.org/10.1093/oxfordjournals.molbev.a003851

SUPPORTING INFORMATION

Additional supporting information can be found online in the Supporting Information section at the end of this article.

How to cite this article: Leong, B. J., Hurney, S., Fiesel, P., Anthony, T. M., Moghe, G., Jones, A. D., & Last, R. L. (2022). Identification of BAHD acyltransferases associated with acylinositol biosynthesis in *Solanum quitoense* (naranjilla). *Plant Direct*, *6*(6), e415. https://doi.org/10.1002/pld3.415